

Microtubule Polymer Assembly and Transport during Axonal Elongation

Sigrid S. Reinsch, Timothy J. Mitchison,* and Marc Kirschner

Department of Biochemistry and Biophysics; and *Department of Pharmacology, University of California, San Francisco, California 94143

Abstract. As axons elongate, tubulin, which is synthesized in the cell body, must be transported and assembled into new structures in the axon. The mechanism of transport and the location of assembly are presently unknown. We report here on the use of tubulin tagged with a photoactivatable fluorescent group to investigate these issues. Photoactivatable tubulin, microinjected into frog embryos at the two-cell stage, is incorporated into microtubules in neurons obtained from explants of the neural tube. When activated by light, a fluorescent mark is made on the microtubules in the axon, and transport and turnover can be visualized directly. We find that microtubules are generated in or near the cell body and continually transported distally as a coherent phase of polymer during axon

elongation. This vectorial polymer movement was observed at all levels on the axon, even in the absence of axonal elongation. Measurements of the rate of polymer translocation at various places in the axon suggest that new polymer is formed by intercalary assembly along the axon and assembly at the growth cone in addition to transport of polymer from the cell body. Finally, polymer movement near the growth cone appeared to respond in a characteristic manner to growth cone behavior, while polymer proximally in the axon moved more consistently. These results suggest that microtubule translocation is the principal means of tubulin transport and that translocation plays an important role in generating new axon structure at the growth cone.

CYTOPLASMIC flux in axons was first demonstrated in the classic experiments of Weiss and Hiscoe (1948) when vesicular elements were found to accumulate at the site of an artificial constriction. Direct visualization of this transport, both in the axon (Burdwood, W. 1965. *J. Cell Biol.* 27:115A; Matsumoto, 1920; Nakai, 1964) and later in isolated axoplasm (Brady and Lasek, 1982; Brady et al., 1982), led to a characterization of vesicular movements as occurring on microtubules in both a retrograde and anterograde manner, and later led to the purification of the proteins responsible for generating these movements (for review see Schroer and Sheetz, 1991; Vale, 1987). Although these studies represent important advances in our understanding of axon growth and function, an equally important and unanswered question is to determine how the structural components of the axon, in particular the microtubules, are formed.

Previous experiments, focusing on the sites of microtubule assembly in the axon, have generated two diametrically opposed explanations of axonal growth (for review see Bamberg, 1988; Hollenbeck, 1989). In one view, based primarily on metabolic labeling studies, microtubules are thought to be assembled in the cell body and transported down the axon (Hoffman and Lasek, 1975). In the other view, based on photobleaching experiments (Lim et al., 1989, 1990; Okabe and Hirokawa, 1990) and local application of microtubule depolymerizing drugs (Bamberg et al., 1986), tubulin is thought to be transported down the axon as monomer and

assembled into microtubules at the growth cone. To resolve this conflict, we have applied the recently developed technique of photoactivation of fluorescence (Krafft et al., 1986; Mitchison, 1989), and a novel method for labeling microtubules in cultured neurons (Tanaka and Kirschner, 1991) with a photoactivatable tag, to study the sites of microtubule assembly in the elongating axon.

By marking axonal microtubules using photoactivation, and following the fate of these marks, we can decide among several models for assembly and transport. For example, if tubulin is transported down the axon as monomer and assembled into microtubules at the growth cone, then the mark on the axonal microtubules would be stationary relative to the cell body and, as a consequence, the mark to growth cone distance would increase. If microtubules are assembled at the cell body and subsequently transported down the axon, then the distance between the cell body to the mark would increase and the mark to growth cone distance would remain fixed. If a specialized transport form of tubulin is transported relative to a stationary array of microtubules (Weisenberg et al., 1987, 1988), the photoactivated mark would split, with one part remaining stationary and the other moving down the axon. This approach can also be used to determine monomer/polymer dynamics along the axon. For example, if exchange between monomer and polymer is rapid, the photoactivated marks would fade rapidly. If exchange is slow and there is an appreciable pool of monomer, there would be rapid partial fading of the labeled zone,

followed by a much slower fading of the remaining signal. There are many possible outcomes predicted by different models that can be tested with this approach.

Using photoactivation, we have shown that during axonal elongation, microtubules are continuously translocated as a coherent phase distally in the axon. By analyzing the translocation rates of microtubule polymer at different distances along the axon we have determined the relative contribution to axonal elongation of different potential microtubule assembly sites along the axon. Our results indicate that assembly at both the cell body and the growth cone contribute significantly to axonal elongation, while microtubule assembly along the axon may at times also contribute to axonal elongation. Furthermore, our results demonstrate that tubulin is transported as polymer, and that this mechanism of transport probably provides most of the subunits required both for microtubule assembly at the growth cone and for microtubule assembly along the axon.

Materials and Methods

Labeling, Incubation, and Plating of *Xenopus* Embryos

Xenopus embryos were fertilized, injected, incubated, and dissected as described in the accompanying paper (Tanaka and Kirschner, 1991) with the following modifications. We used bis-caged fluorescein (C2CF)-labeled bovine brain tubulin (Hyman et al., 1990; Mitchison, 1989) or C2CF-labeled dextran at a concentration of 50 μ M. For plating labeled neural tubes, two protocols were used: (a) explants were cultured as described (Tanaka and Kirschner, 1991); or (b) neural tubes were dissociated by incubation for 5 min in Steinberg's dissociating medium (58 mM NaCl, 0.67 mM KCl, 4.6 mM Tris, pH 7.8–8, 0.4 mM EDTA) before plating, and cultured in RTM (12 mM NaCl, 4 mM KCl, 0.05 mM CaCl₂, 10 mM MgSO₄, 56 mM NaH₂PO₄, 4 mM Na₂HPO₄, 5 mM NaHepes [pH 7.8], 20% L15 with 0.1% gentamycin) supplemented with 1% embryo extract (Harris et al., 1985). All cultures were plated on 40-mm glass coverslips which were sealed with VALAP (vaseline:lanolin:paraffin 1:1:1) over a 35-mm hole drilled in 60 \times 15-mm tissue culture dishes, and then coated with polylysine and complex extracellular matrix (Tanaka and Kirschner, 1991).

Dextran Labeling

All operations were performed at 25°C. Aminodextran, 10 kD, 3.1 amino groups/mol (Molecular Probes, Eugene, OR) was dissolved in dry DMSO at 30 mg/ml. C2CF-SNHS (Mitchison, 1989) was added from a 0.1 M stock in DMSO to give a final concentration of 1.6 mol/mol dextran, followed by triethylamine to the same final concentration. After 1 h, the labeled dextran was precipitated with 5 vol of ethylacetate, and collected by centrifugation (10 kG for 5 min). The dextran was resuspended in DMSO and reprecipitated with ethylacetate. The dextran was then dissolved in aqueous 0.1 M NaHCO₃ and precipitated with 5 vol of ethanol. This step was repeated once more. The final pellet was dissolved in water at 50 mg/ml, cleared by sedimentation at 100 kG for 5 min, frozen in aliquots, and stored at –80°C. The labeling stoichiometry was estimated to be 1.3 C2CF/dextran, and the preparation was free of detectable uncoupled dye as assayed by TLC on silica gel in benzene/acetone/acetic acid 80:20:2. In this system the free dye migrates with an *r*_f of ~0.5, while the dextran remains at the origin.

Microscopy

The experiments were performed using an inverted microscope (model IM35; Carl Zeiss) with modifications for photoactivation and epifluorescence as described previously (Mitchison, 1989). Photoactivation and fluorescence observation were performed using a 100/1.3 phase/neo-fluor objective (Zeiss) and a Hoffman condenser (Modulation Optics, Greenvale, NY), or a Plan APO 60/1.4 oil DM objective (Nikon) and a Nikon phase-contrast 1.25 achromat condenser used as a water immersion condenser. Fluorescent and phase-contrast images were collected with an intensified

silicon-intensified target (ISIT) camera (DAGE-MTI, Michigan City, IN) modified for operation with two independent manual gain controls for phase and for epifluorescence. The ISIT camera was directly mounted on the top port of the microscope. Switching between the two gain controls was controlled by the image processor via a digital input/output (DIO) board (DT2817; Data Translation, Marlboro, MA). The video signal was processed using an IMAGE1 image processing system (Universal Imaging, West Chester, PA). Both trans- and epi-illumination used 100 W halogen light sources. To minimize photodamage and photobleaching, and to allow sequential phase and epifluorescence images to be collected, both light sources were controlled by shutters interfaced to the image processor via the DIO board. The photoactivation set-up was as detailed (Mitchison, 1989). Images were stored using either an Optical Disc Recorder (Panasonic model TQ-2028F) or a MacinStor erasable optical device (Storage Dimensions, San Jose, CA).

Photoactivation and Data Collection

Before photoactivation, the labeled neuronal cell was positioned relative to the irradiation beam, such that the axon lay perpendicular to the irradiation slit. Labeled cells were distinguished from unlabeled cells by a low background fluorescence. The photoactivation beam was applied for a period of 1 s to generate a photoactivation mark ~5 μ m long and spanning the width of the axon. A pair of fluorescence and phase images were collected within 3 s, and then at regular intervals (usually 30 or 60 s). Typically, the fluorescence image used the epifluorescence halogen source at maximum intensity, the ISIT set at about half-maximal gain (constant for a given run but optimized for each axon), with the shutter open for 1 s to collect 32 frames for a summed image. The phase image used the light source at ~25% maximal intensity, the ISIT camera at low gain, and the shutter open for 0.25 s to collect eight frames for a summed image. For visualization of microtubules in the growth cone, cooled charge coupled device (CCD) imaging of *Xenopus* growth cones was carried out as described (Tanaka and Kirschner, 1991). However, total microtubules in C2CF-labeled growth cones were first photoactivated by exposure to a 1-s exposure to the mercury lamp through a Hoechst excitation filter (λ = 360 nm). The low-intensity fluorescein signal required 2-s exposure times.

Detergent Extraction of *Xenopus* Neurons

Xenopus neurons labeled with C2CF-tubulin were photoactivated and phase and epifluorescence images were recorded. Subsequently, 75% of the culture medium was slowly withdrawn and 3/2 vol of microtubule stabilizing buffer (MTSB): 80 mM K-Pipes, pH 6.8, 5 mM EGTA, 1 mM MgCl₂, 0.5% NP-40, containing 20% glycerol, and 10 μ M taxol was carefully added to the culture. Phase and fluorescence images were then recorded.

Image Analysis

Line intensity measurements (see Fig. 4, C and D) and distance measurements (Figs. 5 and 6, C and D) were made using the IMAGE-1 software. For line intensity measurements, the preactivation scan was used to determine the average background intensity along the axon which was mathematically subtracted from subsequent scans. Direct image subtraction was not possible because the neurites are constantly moving in the field. For distance measurements, the peak of intensity was used for the position of the photoactivated mark, and the position of the growth cone neck was determined as described (Tanaka and Kirschner, 1991).

Microinjection and Imaging of C2CF-tubulin in BSC-1 Fibroblasts

BSC-1 fibroblasts were cultured and microinjected as described previously (Schulze and Kirschner, 1986) using an automated pressure injection device (Eppendorf Microinjector 5242; Eppendorf, Fremont, CA). Injected cells were incubated for various amounts of time before labeled microtubules were photoactivated by a 1-s exposure to 360-nm light from the mercury lamp in the epifluorescence light path filtered through a Hoechst excitation filter. Microinjected cells were then permeabilized for 30 s in MTSB to remove soluble tubulin and fixed in MTSB plus 0.5% glutaraldehyde for 10 min at room temperature. Fixed cells were rinsed in PBS, quenched for 6 min in PBS containing 1 mg/ml NaBH₄, rinsed in PBS and were mounted in PBS containing 90% glycerol and 1 mg/ml paraphenylenediamine (Sigma Chemical Co.). Fixed cells were observed with the optical system described above.

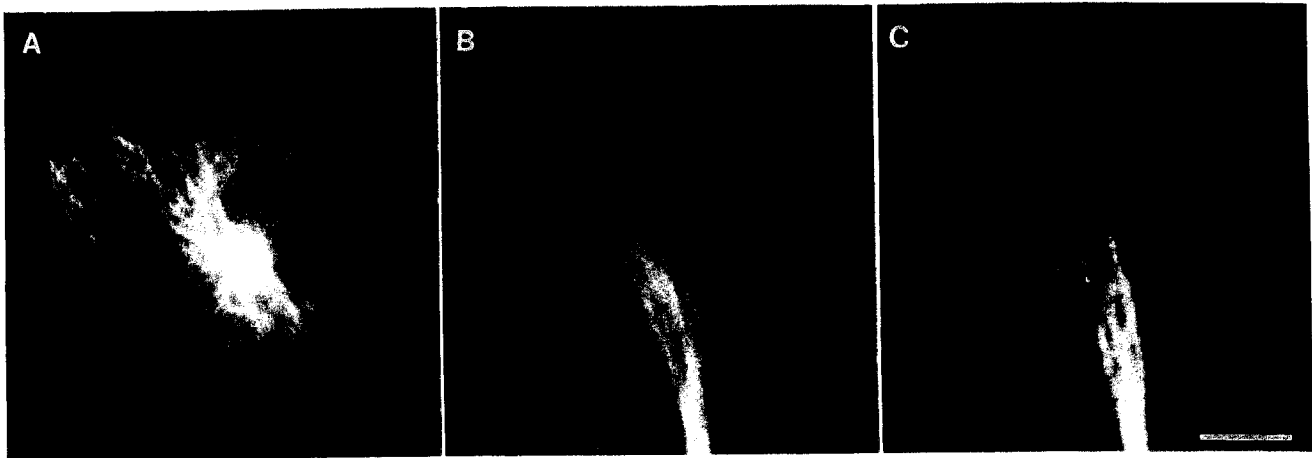


Figure 1. Incorporation of derivatized bovine brain tubulin in cultured fibroblasts and growth cones of labeled *Xenopus* neurons. (A) ISIT image of fluorescein signal in BSC-1 fibroblast microinjected with photoactivatable tubulin, incubated 5 min, then UV photoactivated, permeabilized, and fixed. (B) CCD image of fluorescein signal after UV-photoactivation of live growth cone from *Xenopus* embryo labeled with photoactivatable tubulin. (C) CCD image of rhodamine signal of live growth cone from *Xenopus* embryo labeled with rhodamine tubulin (courtesy of Elly Tanaka). Bars: (A) 20 μm ; (B and C) 5 μm .

Results

Labeling *Xenopus* Neural Tube Axons with Photoactivatable Tubulin

As discussed in the accompanying paper (Tanaka and Kirschner, 1991), it is possible to label the microtubules of primary neurons from the neural tube by injecting derivatized tubulin into cleaving *Xenopus* embryos. This procedure achieves complete labeling of microtubules without perturbing cellular functions as evidenced by the normal development of the embryos. In the following experiments, we have introduced photoactivatable bis-caged-fluorescein-labeled tubulin (C2CF-Tb) into *Xenopus* neuronal cells by the same method, and examined the photoactivated microtubules.

To critically examine the incorporation of photoactivatable tubulin into cellular microtubules, we first chose a cell type with a more favorable morphology, the BSC-1 fibroblast. No microtubules were seen without activation. After activation, typical microtubule arrays with resolution to the level of single microtubules were easily seen (Fig. 1 A). There was no accumulation of fluorescent label in any other part of the cell. When cells were fixed shortly after microinjection, only short fragments of microtubules were visible, most of which were assembled in the periphery of the cell onto the ends of existing microtubules (data not shown). This was an identical result to that observed briefly after injection of biotin-labeled tubulin (Schulze and Kirschner, 1986). Therefore, caged fluorescein behaved indistinguishably from other derivatized tubulin molecules after microinjection into interphase cultured cells.

To determine whether photoactivatable tubulin assembles into the microtubules of neurons, we examined the growth cone, where individual microtubules can be resolved. After photoactivation, individual microtubules can be resolved in the growth cone using a cooled CCD camera, as shown in Fig. 1 B. These images were comparable to those from embryos injected with rhodamine-labeled bovine tubulin (Fig. 1 C), which are discussed in detail in the accompanying pa-

per (Tanaka and Kirschner, 1991). In the rest of the experiments reported in this paper, we have studied microtubules in axons, where their tight packing and overlap makes it impossible to resolve them individually. For these experiments, the lower resolution of the ISIT camera is sufficient to follow the bulk microtubule mass. The loss of resolution is compensated for by the greater effective sensitivity of the ISIT camera, which requires shorter exposure times and lower light intensities than the CCD.

Microtubule Polymer Translocates Distally during Axonal Outgrowth

To examine where microtubules are assembled in elongating axons, we followed the fate of fluorescent marks made by photoactivation in neurons labeled with photoactivatable tubulin. Fig. 2 shows time lapse sequences of two such photoactivation experiments. Phase images (Fig. 2, A and C) and corresponding fluorescence images (Fig. 2, B and D) are shown. In the sequence in Fig. 2 A, the axon grew out of an explanted neural tube, and the growth cone moved from the center of the field to the lower right hand corner, where it was eventually obscured by another neuron. The neuron in Fig. 2 C was an isolated cell in a dissociated culture. Before activation, as shown in the first frame (Fig. 2, B and D), there was a small amount of fluorescent background in the neurons. This background was most likely due to inadvertent photoactivation during incubation or preparation of the culture. In the second frame, a photoactivation mark was made by exposing the cell through a slit projected on the axon. The next three frames show the outgrowth of the axon and the relative position of the activated mark in alternating shuttered phase and epifluorescent images. As the axons elongated, the activated marks translocated distally down the axon. On average, both axons shown in Fig. 2 elongated at 100–120 $\mu\text{m}/\text{h}$. However, the mark in Fig. 2 (A and B) moved at 90–100 $\mu\text{m}/\text{h}$, very close to the rate of growth cone advance, while in Fig. 2 (C and D), the mark moved considerably slower than the growth cone at 68 $\mu\text{m}/\text{h}$.

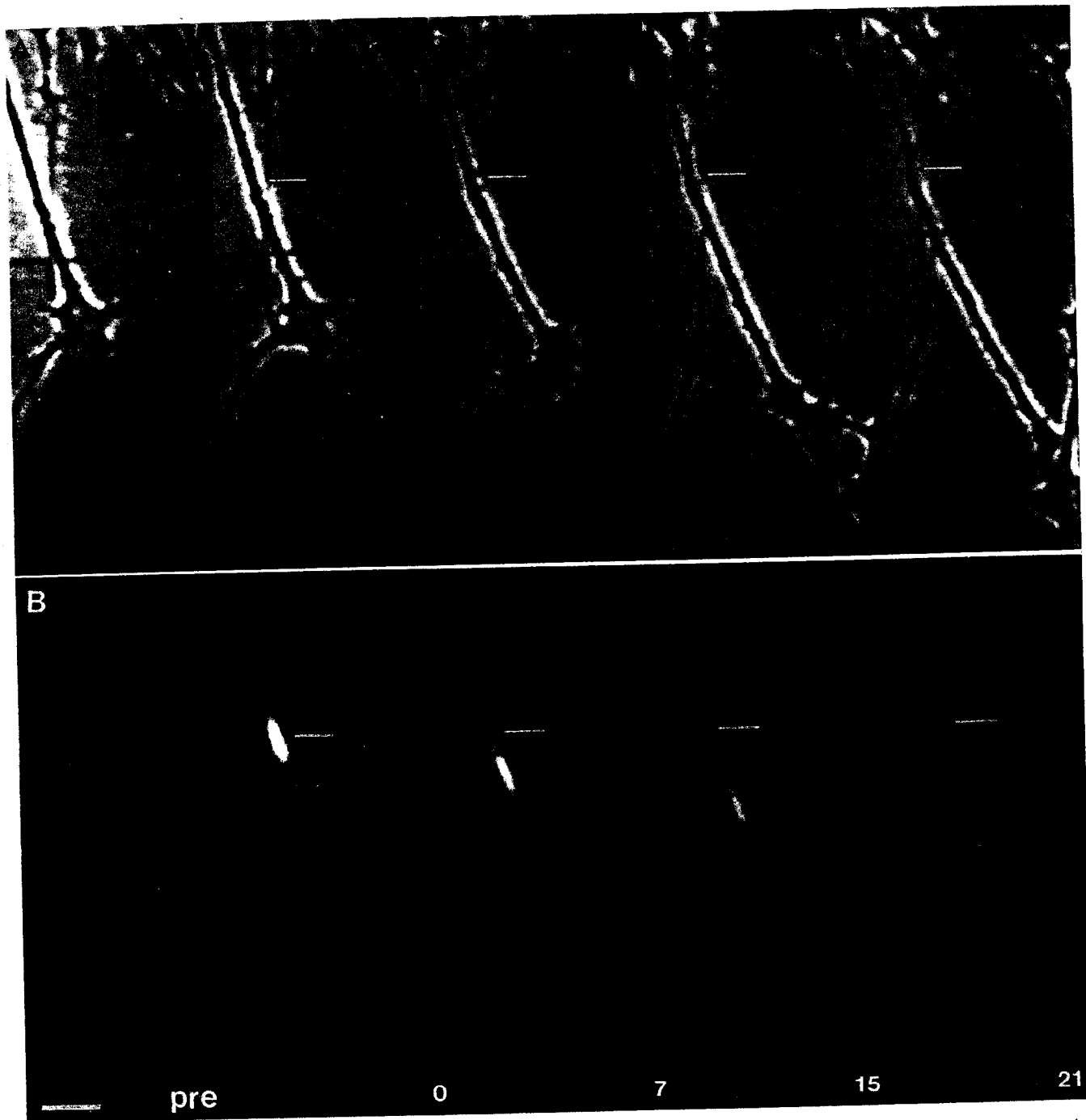


Figure 2. Distal translocation of microtubule polymer in elongating *Xenopus* axons. Phase images (*A* and *C*) and corresponding fluorescein signal (*B* and *D*) before UV photoactivation (*pre*) and at times indicated (minutes) after photoactivation. In *A*, the axon exits the explant at the top and the growth cone grows down and to the right. In *C*, the cells were dissociated before plating and the cell body is out of the frame of the picture. The thin line indicates position of photoactivation mark at $t = 0$. Note that in both sequences, the photoactivated mark translocates distally as the axon elongates behind the growth cone. Bar, 10 μm .

Two characteristics of the position and intensity of the activation marks deserve mention. These characteristics were found in all cells examined in this report. (*a*) No detectable activated signal remained at the site of activation. (*b*) While the intensity of the signal in the mark decreased over time (see a more quantitative treatment for the axon in Fig. 2 *A/B* in Fig. 4 *D*), there was no rapid decrease in the intensity of

the mark, which would be expected if a significant portion of the signal were in monomeric tubulin. 20 s after activation, 90–95% of the signal remained. By contrast, in the mitotic spindle, 50% of the photoactivated signal is lost in 30 s (Mitchison, 1989).

There are inherent limits in the accuracy by which we could estimate the change in the intensity of the fluorescent

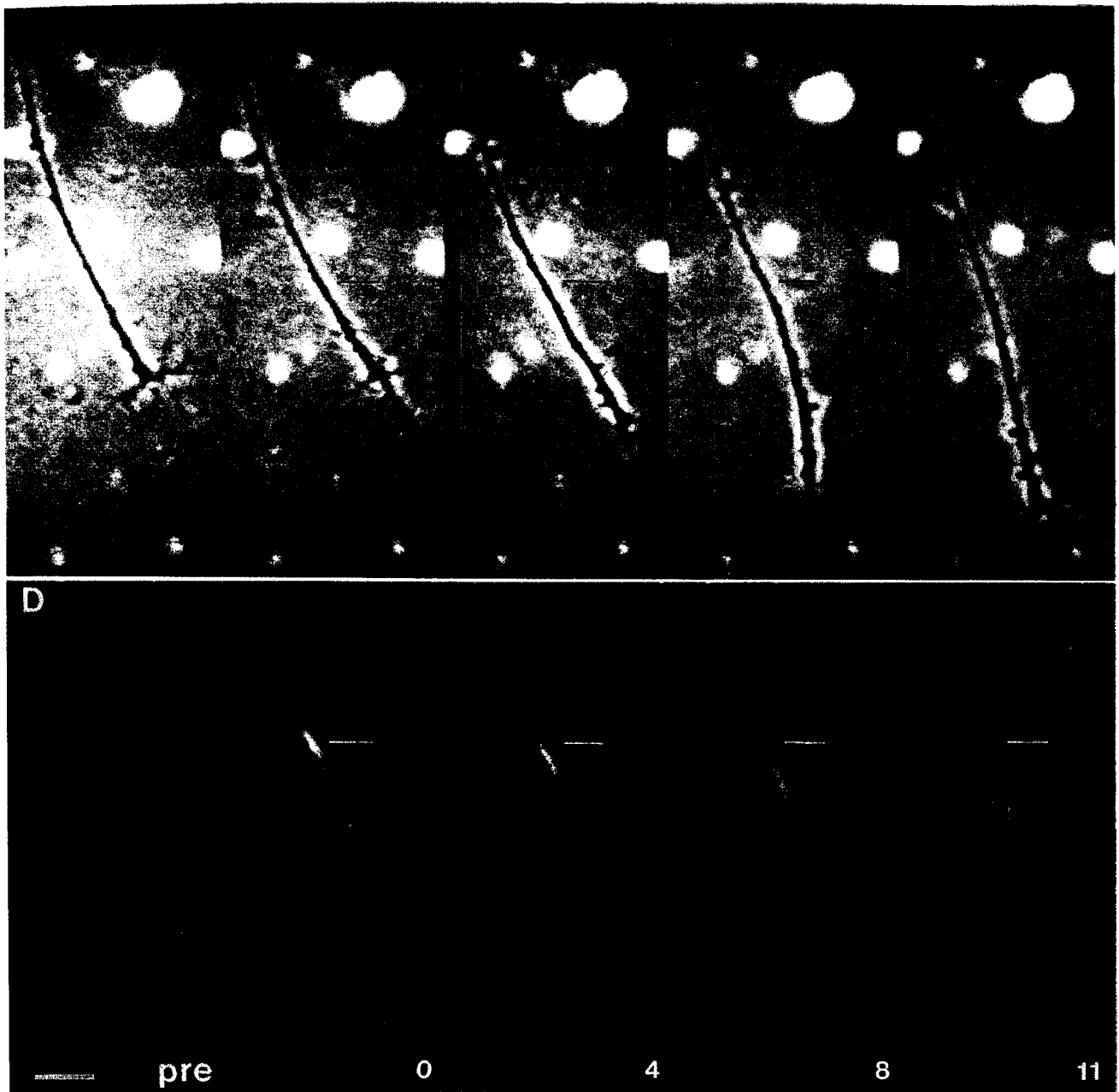


Figure 2.

marks. These limitations come from many sources, such as the nonlinearity of the ISIT camera, fluctuations in the light source, and the nonuniformity of the microscopic field. Nevertheless, we have made an effort to estimate the causes of the loss of intensity with time. In the 21 min between the initial activation and the last frame shown in Fig. 2 (*A* and *B*), the decrease in the integrated intensity of the mark is $\sim 50\%$ (see intensity scan Fig. 4 *D*). We estimate that 35% of the signal loss in this sequence is attributable to bleaching. In separate experiments, we found that 5–10% of the signal was lost in 10-s unshuttered exposures of neurons labeled with photoactivatable tubulin. Since each image in this series represents 32 summed frames for a total of 1-s exposure, and images were collected every 30 s for 21 min, the total exposure is 42 s, and the overall intensity loss due to bleach-

ing in this sequence should be $\sim 35\%$. A second contributing factor was the nonuniformity of the camera field, which is readily visible in Fig. 2 *A*, where the center of the field was brighter than the periphery. Correcting for a uniform background, we can estimate that this contributes $\sim 20\%$ of the gross intensity difference seen in Fig. 2 *B*. Within the accuracy of the measurements, these two contributing factors, bleaching and camera nonuniformity, accounted for most of the decrease in signal.

Is the Moving Signal on Microtubules?

High resolution CCD images of activated tubulin in growth cones indicated that the signal was present as linear elements characteristic of individual microtubules (Fig. 1 *B*). How-

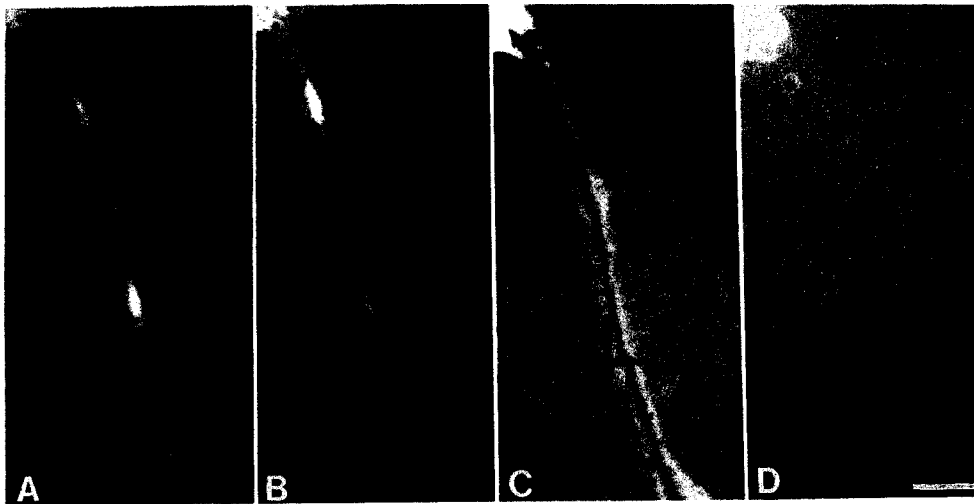


Figure 3. Detergent extraction after UV photoactivation of *Xenopus* neuron labeled with photoactivatable tubulin. Fluorescein signal (*A* and *B*) and corresponding phase images (*C* and *D*) before detergent extraction (*A* and *C*) and after detergent extraction (*B* and *D*) of a neuron labeled with photoactivatable tubulin and photoactivated at two positions along the axon. The field was shifted slightly after detergent extraction so the dark and light intensities in the field of the ISIT camera are not in register between the two sets of images. This caused the photoactivation mark closer to the cell body to appear brighter and the distal mark to appear dimmer after detergent extraction. Bar, 10 μm .

ever, since individual microtubules cannot be resolved in axons, further experiments were necessary to demonstrate that the moving signal we observed was on microtubules rather than in nonpolymeric forms of tubulin. We performed two types of experiments to characterize the nature of the signal. First, neurons labeled with photoactivatable tubulin and subsequently activated were extracted with a nonionic detergent to remove lipid membranes and soluble molecules. Second, we compared the dispersal of the photoactivated tubulin signal with that of a soluble photoactivatable dextran of molecular weight 10,000.

Fig. 3 shows phase and fluorescence images of a neuron with two activated marks before (Fig. 3, *A* and *C*) and after (Fig. 3, *B* and *D*) extraction. Immediately after activation, the cell was permeabilized in a microtubule stabilizing buffer containing taxol, thereby effectively removing all soluble tubulin and membranous organelles, and preserving microtubule polymer. The activated regions in Fig. 3 *A* were still visible in the extracted cell shown in Fig. 3 *B*, while the phase image demonstrates that the extraction markedly lowered the phase density of the image (compare Fig. 3, *C* and *D*). Furthermore, the polymer that remained after permeabilization was very stable under these conditions in the absence of fixation. It was difficult to interpret the intensities of the signals before and after extraction, since the pH and ionic conditions of the milieu directly affect the fluorescence intensity of the fluorophore, and the internal characteristics of the cytosol are unknown.

We compared the loss of intensity of the photoactivatable zone in neurons injected with photoactivatable tubulin with those injected with photoactivatable dextran. As shown in Fig. 4 *A* the dextran signal dispersed almost completely in 104 s. By comparison, in Fig. 4 *B* there was very little spreading or loss of the labeled tubulin in 464 s. Fig. 4, *C* and *D* are scans of the fluorescence intensity versus distance along the axon for the photoactivated dextran and tubulin, respectively, over time. Data from 10 cells confirmed the

qualitative observations; the dextran signal dispersed rapidly (data not shown). By measuring the width at half maximum of the intensity profiles, we calculated the apparent diffusion coefficients for both the dextran and the tubulin, making the formal assumption that both were behaving as diffusible molecules. The calculated diffusion coefficient for the labeled dextran was $2 \times 10^{-8} \text{ cm}^2/\text{s}$, while that for tubulin was $4 \times 10^{-10} \text{ cm}^2/\text{s}$. If we take the dextran behavior as indicative of soluble macromolecules in the axoplasm, then the small apparent diffusion coefficient of tubulin indicates that the tubulin signal must be in an insoluble, presumably polymeric form. Hence, the slow spreading of the tubulin mark most likely has other causes.

The Rate of Microtubule Translocation Varies with Distance along the Axon

Although the rates of microtubule translocation in the axon were often close to the rates of growth cone movement (see, for example, Fig. 2, *A* and *B*), we observed many cases where the translocation rates were significantly slower than that of growth cone advance (Fig. 2, *C* and *D*). In six different experiments of 47 activation marks in 39 neurons, we found that in 46, the polymer advanced a measurable distance over the total observation period. In each experiment, our observation period lasted until the signal decayed to background levels (sometimes up to 45 min), or was obscured by objects in the field. The average rate of growth cone advance in the 39 neurons was $60 \mu\text{m}/\text{h} \pm 37 \mu\text{m}/\text{h}$ (SD) with the fastest moving at $150 \mu\text{m}/\text{h}$. The tubulin polymer moved at $38.5 \mu\text{m}/\text{h} \pm 31.4 \mu\text{m}/\text{h}$ (SD), with the fastest moving at $117 \mu\text{m}/\text{h}$. Therefore, on average, the growth cone advanced faster than the rate of microtubule translocation.

We suspected that there might be a relationship between the distance from the cell body and the relative rate of forward advance. Since many of our measurements were made on axons growing out of neural tube explants where the posi-

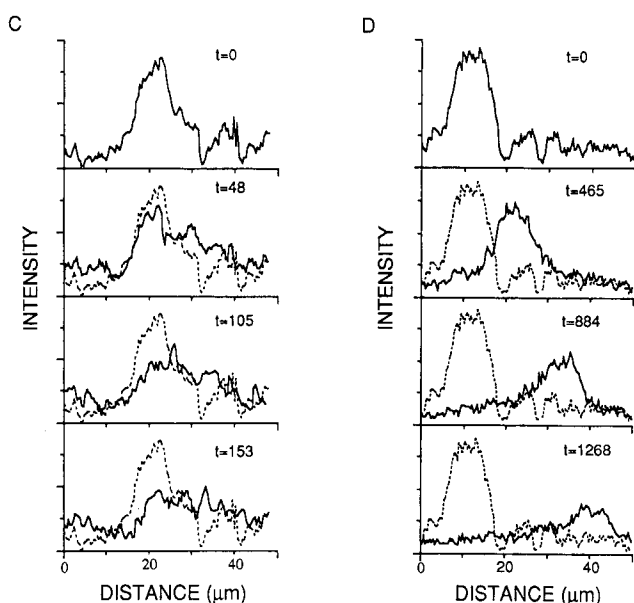
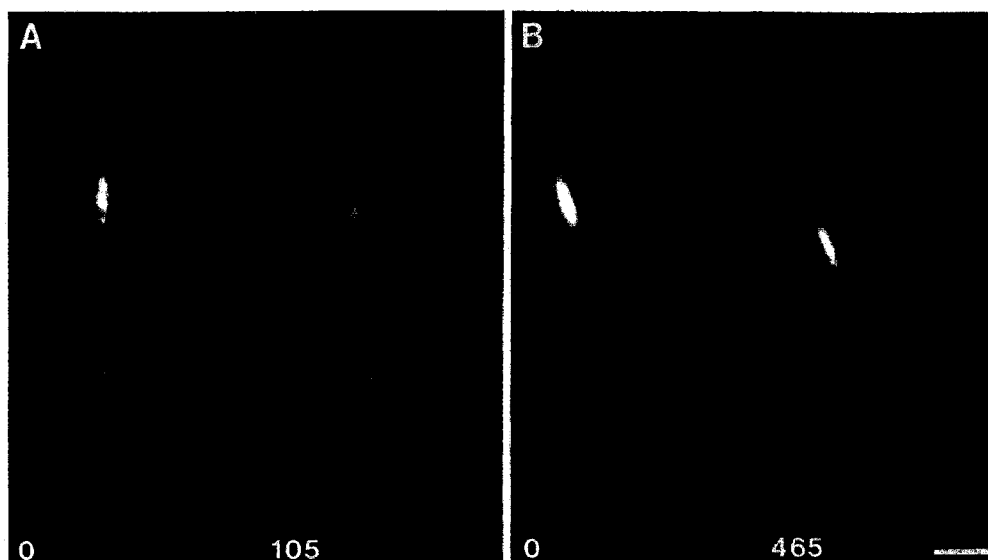


Figure 4. Comparison of the kinetics of diffusion of photoactivatable dextran with photoactivatable tubulin in *Xenopus* neurons. Fluorescein signal immediately after photoactivation and at times (in seconds) indicated for photoactivatable dextran (*A*) and photoactivatable tubulin (*B*). The dextran signal spread throughout the axon and almost returned to a preactivation level after 105 s, while the tubulin spread only minimally and decreased in intensity by 30% after 465 s. (*C* and *D*) Digitization of dextran and tubulin sequences over longer times matching frames in *A* and *B*, respectively. The solid line is the fluorescein intensity at indicated times (in seconds) and is superimposed onto the fluorescence intensity immediately following photoactivation (*dotted lines*). Abscissa is the distance from defined point on the axon proximal to the photoactivated region, so movement of photoactivated tubulin signal is towards the growth cone. Bar, 10 μm .

tion of the cell body was difficult to identify, we correlated the rate of movement of the photoactivated mark with the distance from the growth cone. As shown in Fig. 5, in neurons where the distance between the mark and the growth cone was less than 15 μm (Fig. 5, *solid bars*), 43% of the marks moved at rates that were at least 80% of the rate of growth cone advance (pool 0.8–1.0 plus pool >1.0). In neurons where the activated mark was further than 15 μm from the growth cone (Fig. 5, *open bars*), only 14% of the marks moved at rates that were 80% or greater than the rate of axon elongation; 50% of the marks moved at rates that were <40% of the rate of growth cone advance (pool 0–0.2 plus pool 0.2–0.4). It is important to note that microtubule translocation occurred at all positions along the axon, even very close to the cell body, and that at all levels the polymer seemed to move as a coherent unit. Furthermore, microtubule polymer movement continued in the absence of axonal elongation in 3 out of 46 neurons (see Fig. 8).

The Rate of Microtubule Movement at Different Positions within Single Axons

Pooled data indicated that the rate of polymer movement might vary with distance from the cell body within an individual axon. To follow the fate of microtubules at different positions along single axons, we made multiple activation marks on dissociated neurons where both the cell body and the growth cone were visible. Fig. 6 (*A* and *B*) shows frames of two of seven neurons that we studied with multiple activation marks. In Fig. 6 (*C* and *D*) we show plots of the positions of the growth cone and the individual marks as a function of time for each experiment. In the neuron in Fig. 6 *A/C*, all three activated regions, at 0.48, 0.69, and 0.83 (distance from the cell body relative to the total axon length), moved out from the cell body at the same overall rate of 21 $\mu\text{m}/\text{h}$. As the axon elongated, the growth cone (*dotted line*) advanced away from the distal-most mark, and continued to advance

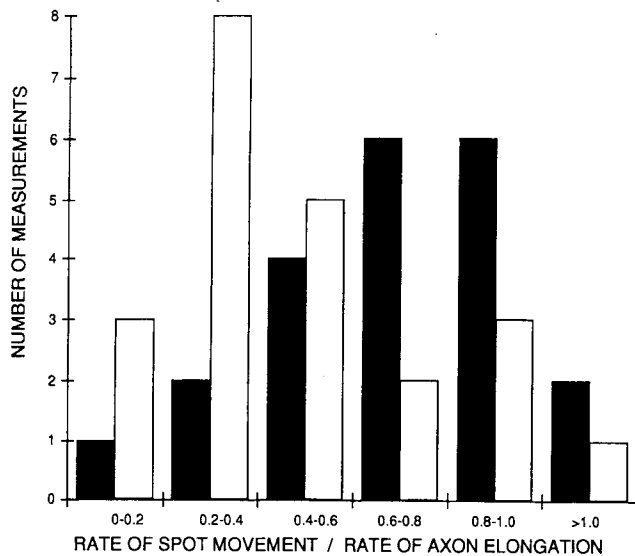


Figure 5. Ratio of polymer translocation rates to corresponding growth cone advance rates as a function of the distance from the growth cone. The rate of polymer translocation was divided by the rate of advance of the neck of the growth cone (see Materials and Methods). Two pools were compared: neurons where photoactivations were made within 15 μm of the growth cone (filled bars; $n = 21$) and neurons where photoactivations were made greater than 15 μm from the growth cone (open bars; $n = 22$). Note that marks made closer to the growth cone moved faster than marks made greater than 20 μm from the growth cone.

at an overall rate 2.6 times the rate of microtubule translocation. Neither the growth cone nor the polymer advanced in a smooth fashion, rather, both showed saltatory advance, which was especially notable in the growth cone.

The second neuron (Fig. 6 B/D) displayed a rather different polymer behavior. In this case, while all three marks moved away from the cell body, the relative distances between the marks also increased, as did the distance from the distal-most mark to the growth cone. Therefore, the microtubule polymer moved at different rates at different positions in this axon. The spot closest to the cell body, at a relative position of 0.47, moved at the slowest rate (10.2 $\mu\text{m}/\text{h}$), while the spot closest to the growth cone, at a relative position of 0.94, moved at the fastest rate (40.2 $\mu\text{m}/\text{h}$). This fast rate was still slower than the overall rate of growth cone advance (66 $\mu\text{m}/\text{h}$). While the two marks closest to the cell body advanced steadily, the mark closest to the growth cone seemed to reflect the saltatory growth cone behavior. Changes in the rate of polymer movement in the distal-most mark sometimes preceded changes in the rate of growth cone movement, while at other times changes in the rate of polymer movement lagged behind those of the growth cone. For example, in the first 2.5 min, the distal mark moved at a faster rate (72 $\mu\text{m}/\text{h}$) than the growth cone (12 $\mu\text{m}/\text{h}$). During the next 10 min, the distal mark slowed to 12 $\mu\text{m}/\text{h}$, while the growth cone advance rate reached 156 $\mu\text{m}/\text{h}$. At 13 min, the distal mark began to move at this faster rate, and for the rest of the time course followed the growth cone rate very closely.

Plots of life histories of all of these multiply marked neurons indicated that there were differences in polymer behavior along the proximo-distal axis. In general, polymer close to the cell body moved slower and at a more consistent

rate than polymer close to the growth cone. Yet as shown in Fig. 6 (A and C), in some cells marks made at different positions along the axon can move together. At all positions along the axon the polymer moved as the growth cone advanced.

Behavior of Microtubule Polymer Near the Growth Cone

Over the long term, there must be a correlation between the advance of the growth cone and the growth of the cytoskeleton behind it. As discussed above, while the rate of microtubule advance along the axon is fairly uniform, near the growth cone the rate of polymer movement can display more rapid changes. We have examined, in greater detail, the relationship between microtubule advance near the growth cone, and the behavior of the growth cone for 21 neurons in which activation marks were made within 20 μm of the growth cone. We have found that this behavior falls into three categories, all of which a single neuron can possess at different times.

In the first category, shown in Fig. 7 A, the growth cone advanced with a fairly uniform morphology (this is also true of the growth cone in Fig. 2 A). As the growth cone advanced (Fig. 7 C), both the neck (Fig. 7, *dotted line*) and the distal tip of the growth cone also advanced; the microtubule polymer (Fig. 7 B) moved at a rate similar to that of the growth cone. The distance between the photoactivated mark on the microtubule polymer (Fig. 7 C, *arrow*) and the neck of the growth cone (Fig. 7 C, *dotted line*) remained fairly constant. The rate of polymer advance (102 $\mu\text{m}/\text{h}$) in this instance slightly exceeded the rate of growth cone advance (74 $\mu\text{m}/\text{h}$). This coupling of microtubule polymer advance with growth cone advance was seen in 17 out of 21 neurons that moved at very different rates. We termed this behavior coupled elongation/translocation.

In the second category shown in Fig. 8, the growth cone paused temporarily and polymer movement continued. When both the distal tip and the growth cone neck stalled (Fig. 8, A and C), we found that microtubule advance often continued (Fig. 8, B and C). In this instance, the distance (Fig. 8 C, *double headed arrow*) from the activated mark (Fig. 8 C, *arrow*) to the neck of the growth cone (Fig. 8 C, *dotted line*) decreased as the microtubules advanced toward the growth cone. In this neuron and others, we noted an increase in the phase density within the growth cone. For example, in the last panel of Fig. 8 A there is a prominent phase-dense region that appears to hook to the left. We interpret this to be a bundle of microtubules and associated organelles that moved into and filled up the growth cone with microtubule polymer as the microtubule polymer advanced (see related descriptions in Tanaka and Kirschner, 1991). This sequence is a good example of continuous microtubule polymer movement into the growth cone in the complete absence of growth cone advance; a condition which we term extrusion.

In the third category, shown in Fig. 9, the proximal part of the growth cone membrane collapsed and that region of the growth cone was converted into new axon, a process we call conversion (Mitchison and Kirschner, 1988). During conversion (Fig. 9 A), the distal tip of the growth cone paused while collapse of the membrane behind it had the effect of advancing the neck of the growth cone (Fig. 9 C, *dotted line*), while a new segment of axon formed behind the neck. In this condition, the forward translocation of the microtubule poly-

mer also paused (Fig. 9 B) and, as a consequence there was a rapid increase ($12 \mu\text{m}/133 \text{ s} = 324 \mu\text{m}/\text{h}$) in the distance from the mark to the growth cone. After conversion was complete, the growth cone and microtubules advanced together again, as shown in the last panel of Fig. 9 (A and B). We observed this process of growth cone conversion in 8 of 21 neurons.

Discussion

The Properties of Photoactivated Microtubules in the Axon

The interpretation of the photoactivation experiments depends on whether the photoactivatable probe remains on tubulin, whether that tubulin is functional, and whether we can assess if it is on monomer or polymer. Bulk chemical methods for characterizing the labeled tubulin in the embryo would be of little value because the derivatized tubulin may be handled differently in different cell types in different regions of the embryo. Instead, we have had to base our analysis on the physical and functional properties of tubulin that we can glean from observation in the specific cells that we are studying.

In growth cones, photoactivated tubulin was visible as linear polymers of uniform intensity and caliber (Fig. 1 B). These images were similar to those seen with rhodamine labeled tubulin (Fig. 1 C). Even though we cannot resolve individual microtubules in the axon because of overlap, it is likely that the photoactivatable signal in the axon is also present on polymer, some of which is presumably continuous with microtubules in the growth cone.

Several features of the photoactivatable signal in axons suggest that it is present primarily on polymer. First, at all points along the axon the fluorescent mark translocated coherently without leaving a significant trailing signal at the site of photoactivation (Figs. 2, B and D, 6, A and B, 7 B, 8 B, 9 B). Second, significant signal remained after detergent extraction which should solubilize all monomer (Fig. 3). Finally, the slow spreading of the photoactivated mark was unlike that expected for soluble tubulin. These will be discussed below.

The coherence of the signal through transport has several implications. If the axon contained a transport form of tubulin that was separate from a stationary polymeric form (Weisenberg et al., 1987, 1988), the signal would be expected to split into two phases, a stationary polymer phase and a moving transport phase. Since we could detect no separation of the signal into two phases, most of the signal must therefore be on one form of tubulin. Alternatively, if there is a transport form other than polymer, then the transport form and the axonal polymer must be translocating together.

Most of the signal cannot be due to monomer since monomeric tubulin would be expected to diffuse relative to microtubules, and the fluorescent signal again should have split into two components, a diffusible component representing the soluble tubulin that spread isotropically and a nondiffusible component representing the microtubule polymer that could have either been stationary or could have translocated. Our analysis of the intensity data at short time points after photoactivation rules out the existence of such a diffusible phase consisting of $>10\%$ of the total tubulin. In addition,

we used photoactivatable dextran of slightly smaller Stokes radius than monomeric tubulin to measure diffusion in the axon (Fig. 4, A and C). We calculated an apparent diffusion coefficient for this photoactivatable dextran; it behaved as a soluble component in a medium of about 10 times the viscosity of water, a value similar to that observed for the diffusion of dextran in other cells (Lang et al., 1986; Luby-Phelps et al., 1986). The photoactivated tubulin behaved very differently. If we estimate the apparent diffusion coefficient for tubulin based on the spreading of the photoactivatable zone, it was 50 times slower than the dextran, corresponding to the free diffusion in the cell environment of a molecule of 10^{10} D, a particle larger than a centriole. Most likely the signal is not diffusing at all, and the slow spreading of the fluorescent mark is due to some other mechanism such as sliding (see below). These properties of the photoactivated tubulin in the axon: nonextractability, coherence through transport, and non-diffusibility are all characteristics of polymer and not monomer.

Microtubule Assembly in Axons

The vectorial movement of tubulin polymer from the cell body towards the growth cone is the predominant feature of microtubule behavior in the axons that we have studied. Overall microtubules translocated throughout the axon at a slower rate ($38.5 \pm 31.4 \mu\text{m}/\text{h}$) than that of growth cone advance ($60 \pm 37 \mu\text{m}/\text{h}$). Furthermore, polymer nearer the cell body moved slower than polymer near the growth cone (Figs. 5 and 6, C and D). These three observations, vectorial transport of polymeric tubulin, a gradient in the rate of polymer movement as a function of distance from the cell body, and the more rapid rate of growth cone advance must be explained in terms of the sites of microtubule assembly, the number of microtubules in the axon, and the mechanisms and rates of microtubule translocation.

Microtubule assembly in or near the cell body is strongly supported by these photoactivation experiments. The coherent vectorial movement of polymeric tubulin as close as $15 \mu\text{m}$ to the cell body requires that tubulin polymer must be generated already at this level. The movement of the photoactivated zones cannot be due to a general elastic expansion of the axon, since translocation can occur in the absence of axon growth (Fig. 8). The movement in multiply marked axons is also incompatible with elastic expansion; in some cases all of the marks moved as a coherent unit (Fig. 6, A and C). Assembly of microtubules in or near the cell body and vectorial transport of tubulin polymer down the axon is supported by metabolic pulse-labeling experiments in many neuronal cell types in vivo (Hoffman and Lasek, 1975; Lasek et al., 1984) and in vitro (Black, 1986).

The separation of the photoactivated marks in some of the multiply marked neurons could have two explanations. Microtubules could be telescoping out in the neuron, causing the microtubule density to decrease with the distance from the cell body. There is some evidence that microtubule number is in fact greater in the proximal axon than in the distal axon (Bray and Bunge, 1981; Letourneau, 1982). Alternatively, the microtubules could telescope out, but the density could be held constant by intercalary assembly onto the ends of microtubules along the axon from a pool of monomer. Assembly along the axon has support from experiments using

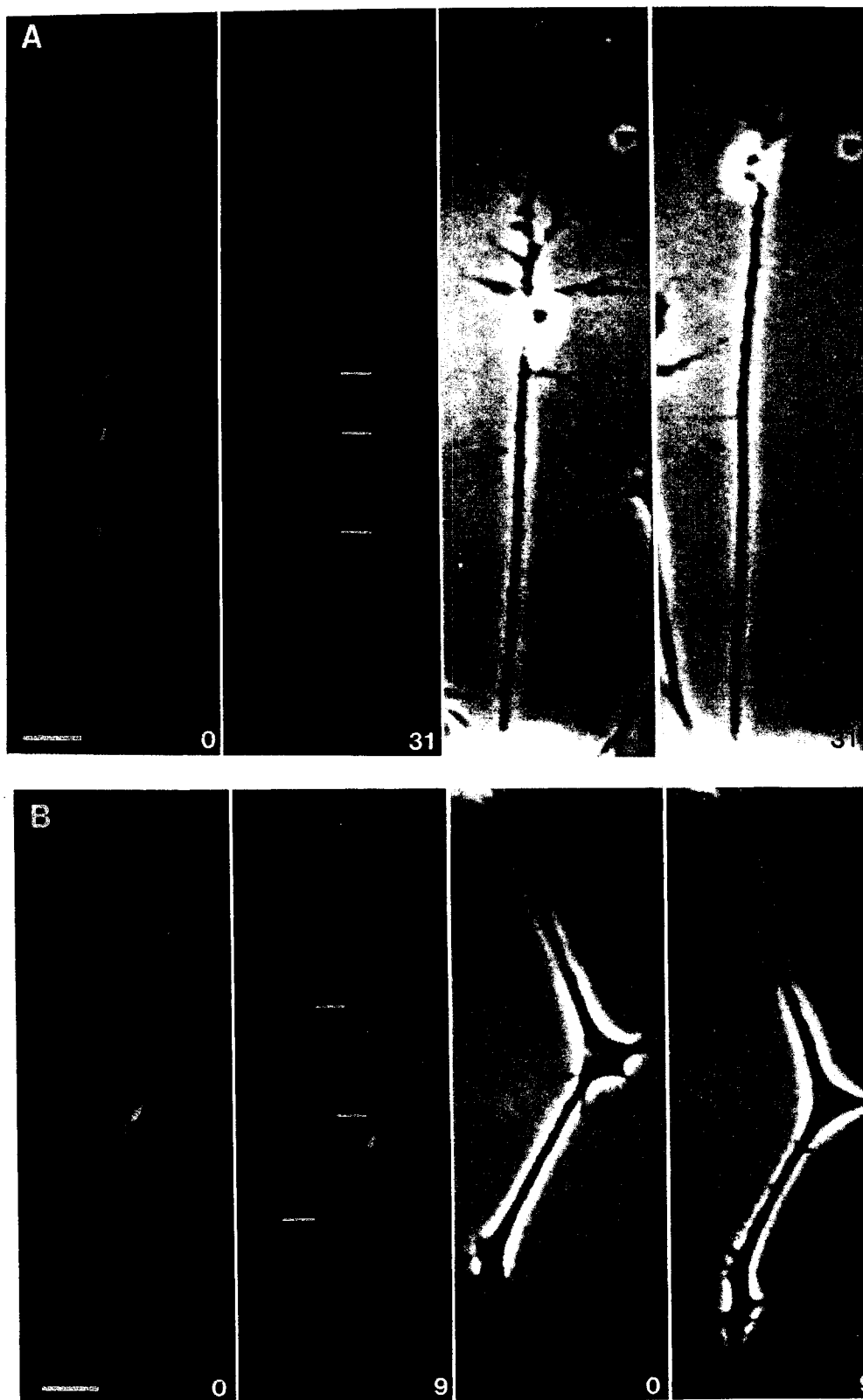


Figure 6. Multiple photoactivations in two neurons. (*A* and *B*) Fluorescein signal (*left panels*) and corresponding phase images (*right panels*) immediately after photoactivation and at the indicated times (minutes) in *Xenopus* neurons labeled with photoactivatable tubulin. The thin lines indicate the positions of the marks immediately after photoactivation. (*C* and *D*) Life histories of the photoactivation marks and growth cone movements matching the neurons shown in *A* and *B*. The distances of the marks from the cell body immediately after photoactivation; (*A* and *C*) proximal mark (●) 37.3 μm ; middle mark (▲) 53.3 μm ; distal mark (◆) 63.7 μm ; and the growth cone (*dashed line*) 77.0 μm . (*B* and *D*) Proximal mark (●) 46.9 μm ; middle mark (▲) 69.1 μm ; distal mark (◆) 93.5 μm ; and the growth cone (*dashed line*) 99.2 μm . Note how the marks in *A* and *C* track together while those in *B* and *D* separate during axonal elongation. Bar, 10 μm .

microinjection (Keith and Blane, 1990; Okabe and Hirokawa, 1988), photobleaching (Lim et al., 1990; Okabe and Hirokawa, 1990) and immunohistochemical (Baas and Black, 1990; Lim et al., 1989) approaches. However, the monomeric subunits driving this assembly would ultimately have

to come from the cell body, and would have to move down the axon by diffusion, as discussed below. We cannot distinguish between these two mechanisms of extension of the axonal microtubule cytoskeleton. However, a slow telescoping of the microtubules, with or without intercalary assembly, is

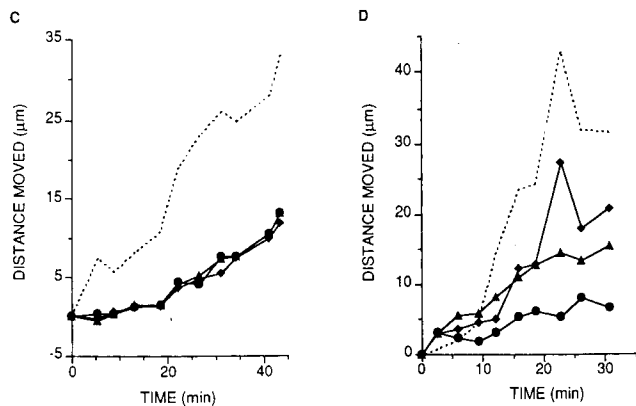


Figure 6.

the most likely explanation for the broadening of the photoactivatable zones. For example in Fig. 6 B, the distal mark moved $30\ \mu\text{m}$ while the proximal mark moved $25\ \mu\text{m}$, producing a 20% increase in extension of the intervening microtubules in the axon. During this time, the individual zones broadened $\sim 30\%$. Thus, both the length of the zones and the distance between them increased in similar proportions, suggesting that the same process, telescoping, with or without intercalary assembly, was responsible.

Near the growth cone, photoactivatable marks often moved at rates comparable to that of the growth cone. However, in most cases the growth cone moved faster than the movement of the mark, suggesting either a drastic thinning of microtubules near the growth cone, or new assembly with subunits presumably provided either by diffusion or by depolymerization of microtubules in the axon. Tanaka and Kirschner (1991) have observed apparent elongation of microtubules in the growth cone. However, it is difficult to resolve the relative contributions of forward translocation and assembly to microtubule elongation. Assembly at the growth cone is supported by immunohistochemical (Baas and Black, 1990; Lim et al., 1989) drug inhibition (Bamburg et al., 1986) and photobleaching studies (Lim et al., 1990; Okabe and Hirokawa, 1990). For the relatively short neurons studied here, there would be no difficulty for subunits to be provided to the growth cone by diffusion. Microinjection experiments of derivatized tubulin in cultured pheochromocytoma cells and dorsal root ganglion cells in vitro have suggested that diffusion is sufficient to bring subunits to all regions of the cell body and axon (Keith, 1987; Keith and Blane, 1990; Lim et al., 1989; Okabe and Hirokawa, 1988), where they can be incorporated into microtubules. These cells have short processes, where diffusion of subunits throughout the cell can occur in seconds or minutes. However in axons longer than 1 mm, diffusion would not accomplish appreciable transport of tubulin within a day. Therefore, the physical limitations of diffusion argue strongly for some mechanism of tubulin transport in long axons. The pulse-labeling experiments and our direct visualization of vectorial transport of microtubules argue that such a mechanism exists and that it comprises polymer assembly in the cell body or in the proximal axon and its subsequent movement down the axon. For long axons, translocation would be the only practical known means of axonal growth.

Microtubule Translocation and Growth Cone Behavior

Using photoactivation, we have correlated the translocation of microtubules in the axon just proximal to the growth cone with the movements of the growth cone and noted three general patterns of behavior: (a) coupled elongation/translocation, during which the polymer moves at virtually the same rate as growth cone; (b) extrusion, during which the growth cone slows, pauses or stops altogether and the polymer continues to move forward; and (c) conversion, during which the polymer pauses as the proximal region of the growth cone collapses to form a new segment of axon. We believe that these three polymer behaviors that we observed near the growth cone are related to the three different microtubule distributions that are generated in the growth cone (Tanaka and Kirschner, 1991). During coupled elongation/translocation (Fig. 7), the rate of microtubule polymer translocation equals that of growth cone advance. In this situation, microtubules may advance as a splayed array. During extrusion (Tanaka and Kirschner, Figs. 6 and 8; this manuscript, Fig. 8), the rate of polymer translocation exceeds that of growth cone advance. As a result, axonal microtubules may move into the growth cone. When this mass of extruded microtubules collides with the growth cone margin, we imagine that looped arrays would be formed. During conversion (Fig. 9), the growth cone may contain a dense array of looped microtubules which compresses into a bundle proximally and straightens distally. The corresponding event is seen in detail by Tanaka and Kirschner (1991). Though there is a complementarity between the direct visualization of microtubules and photoactivation of tubulin, neither method allows us yet to estimate accurately the relative contribution of microtubule polymerization and forward translocation to the formation of new microtubules in the growth cone.

The Interpretation of Photobleaching and Other Experiments

Three previous experiments using photobleaching of rhodamine-labeled microtubules in pheochromocytoma cells (Lim et al., 1989; Okabe and Hirokawa, 1990) and dorsal root ganglion cells (Lim et al., 1990) failed to find any evidence for vectorial flow, and concluded that axons assemble by adding subunits at the growth cone. (However, see also Keith who found support for axonal transport of tubulin in photobleached axons [Keith, 1987].) The simplest explanations for the failure of the photobleaching experiments to find vectorial transport, is that the cells used in those experiments had much different behavior from the *Xenopus* neurons or that the experimental methodologies of photobleaching experiments emphasized features different from the photoactivation experiments.

The primary cultured neurons from *Xenopus* neural tube explant cultures grew 5 to 30 times more rapidly than the cell types used in the photobleaching experiments; hence the precision of measuring movement was greater in the photoactivation experiments. However, the types of translocation found in the *Xenopus* neurons should have still been observable if this process occurred in these cell types. The experimental differences that might account for the discrepancies concern the sensitivity of photobleaching and photoactivation to different kinetic properties of monomer-polymer systems. Pho-

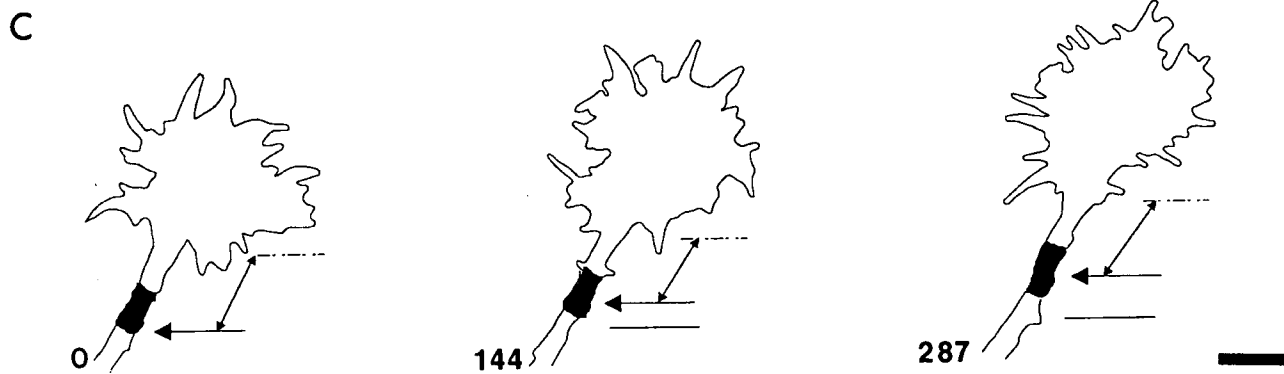
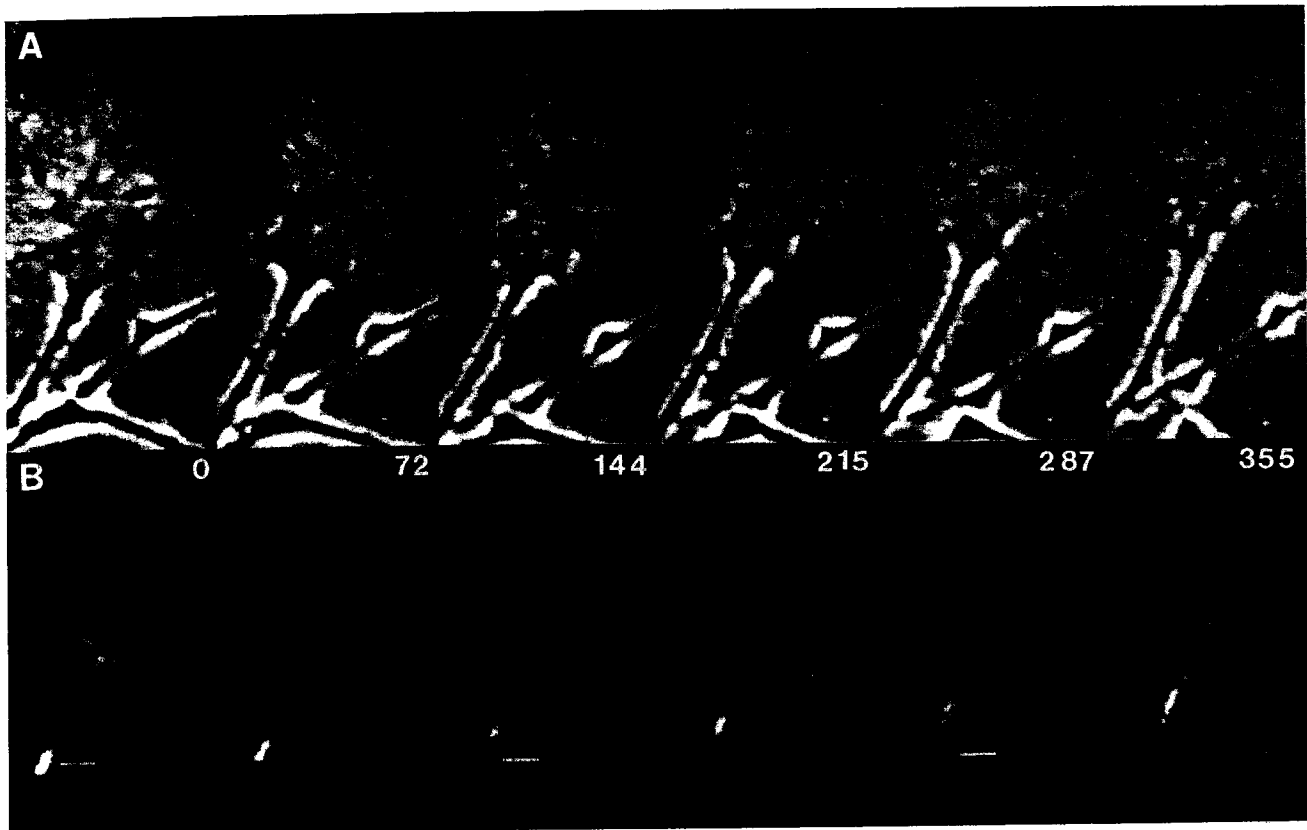


Figure 7. Coordination of polymer movement with growth cone movement: coupled elongation/translocation. Phase images (A) and corresponding fluorescein images (B) at the times indicated (minutes) after photoactivation. (C) Tracing with superimposed fluorescein signal and phase outline of the growth cone from panels 1, 3, and 5. Note that distance (\leftrightarrow) between photoactivation mark (arrow) and the neck of the growth cone (dashed line) remains fairly constant. Solid line shows starting position of photoactivation mark in B and C. Bar, 10 μm .

photoactivation is most sensitive to the slowest exchanging component of a complex system and has been successfully used to demonstrate the poleward flux of kinetochore microtubules during metaphase *in vivo* (Mitchison, 1989), and in spindles assembled *in vitro* (Sawin and Mitchison, 1991). Photoactivation experiments detected this poleward movement, while photobleaching experiments did not (Gorbsky and Borisy, 1989; Gorbsky et al., 1987).

A problem that has plagued all fluorescence experiments is photodamage. In general, photoactivation has advantages over photobleaching since the light energy (number of photons) required to photoactivate a caged fluorophore molecule

is several orders of magnitude less than that required to photobleach a fluorophore. During photobleaching, oxygen radicals are produced which can damage cells. The total amount of light energy absorbed by the cell during the observation period is much less with photoactivation since only the photoactivated, rather than the total, labeled tubulin is fluorescent. Other potential targets for photodamage are putative microtubule motors which have been shown to be very sensitive to photodamage. For example, purified kinesin and dynein are irreversibly inactivated when subjected to light in the presence of fluorescently labeled microtubules *in vitro* (R. Vale, personal communication). Therefore, if microtu-

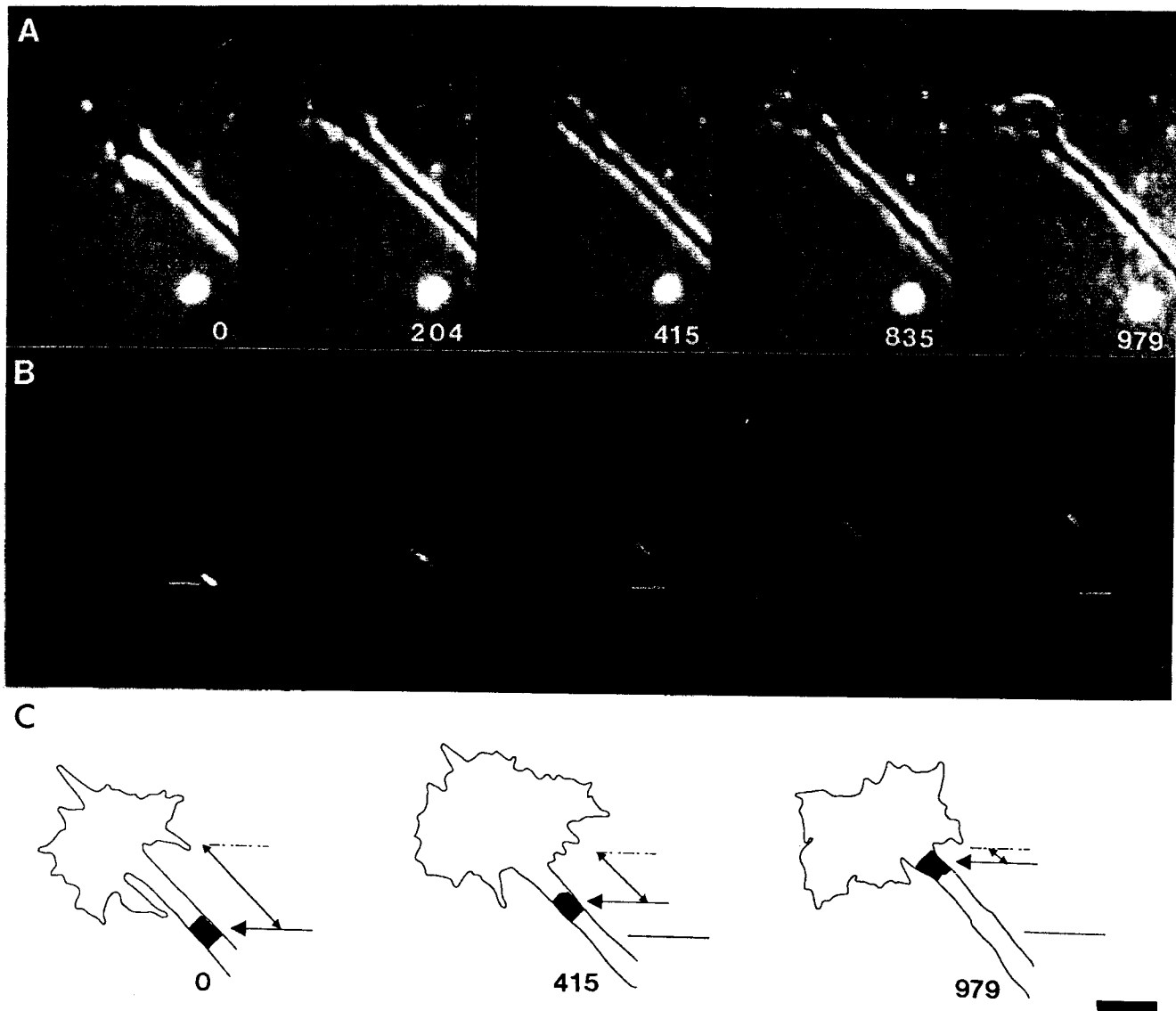


Figure 8. Coordination of polymer movement with growth cone movement: extrusion of polymer. Phase images (*A*) and corresponding fluorescein images (*B*) at the times indicated (minutes) after photoactivation. (*C*) Tracing with superimposed fluorescein signal and phase outline of the growth cone from panels 1, 3, and 5. Note that the growth cone advance stops and the distance (\longleftrightarrow) between the photoactivation mark (arrow) and the neck of the growth cone (dashed line) decreases indicating continued polymer movement in the absence of growth cone advance. Solid line indicates starting position of photoactivation mark. Bar, 10 μm .

bule motors are required for microtubule translocation in the axon, local photobleaching might damage such a motor without causing any detectable ultrastructural changes.

The Mechanism of Microtubule Translocation

The coherence of the photoactivatable spots on microtubules suggests that the microtubules are linked together. Cross-bridges that may be involved in microtubule bundling have been detected between components of the cytoskeleton in axons (Hirokawa, 1982; Hirokawa et al., 1988; Hirokawa and Yorifuji, 1986). Though bundling seems to be an early event in the conversion of the microtubule array in growth cones to that of the axon in these neurons (Tanaka and Kirschner, 1991), it is not clear whether the microtubules are strongly cross-linked. The spreading of the photoactivatable marks in multiply activated axons and the broadening of each

photoactivatable zone suggests that microtubules may move relative to one another. However, though an activity which causes microtubule sliding in vitro has been purified from brain (Shpetner and Vallee, 1989) and microtubule sliding is implicated in Teleost cone elongation (Gilson et al., 1986; Warren and Burnside, 1978), the evidence for sliding of microtubules in the axon is still conjectural (Lasek, 1986) and demands a more quantitative and direct study.

What powers the vectorial transport of microtubules in the axon? Since microtubule transport continues in the absence of axonal growth, membrane expansion at the growth cone cannot be responsible for drawing microtubules towards the growth cone. It also seems unlikely to us that neurons can act like toothpaste tubes, where a process restricted to the cell body could exert a force that would drive microtubule movement at long distances. A microtubule-based mechanochemical motor working along the sides of microtubules,

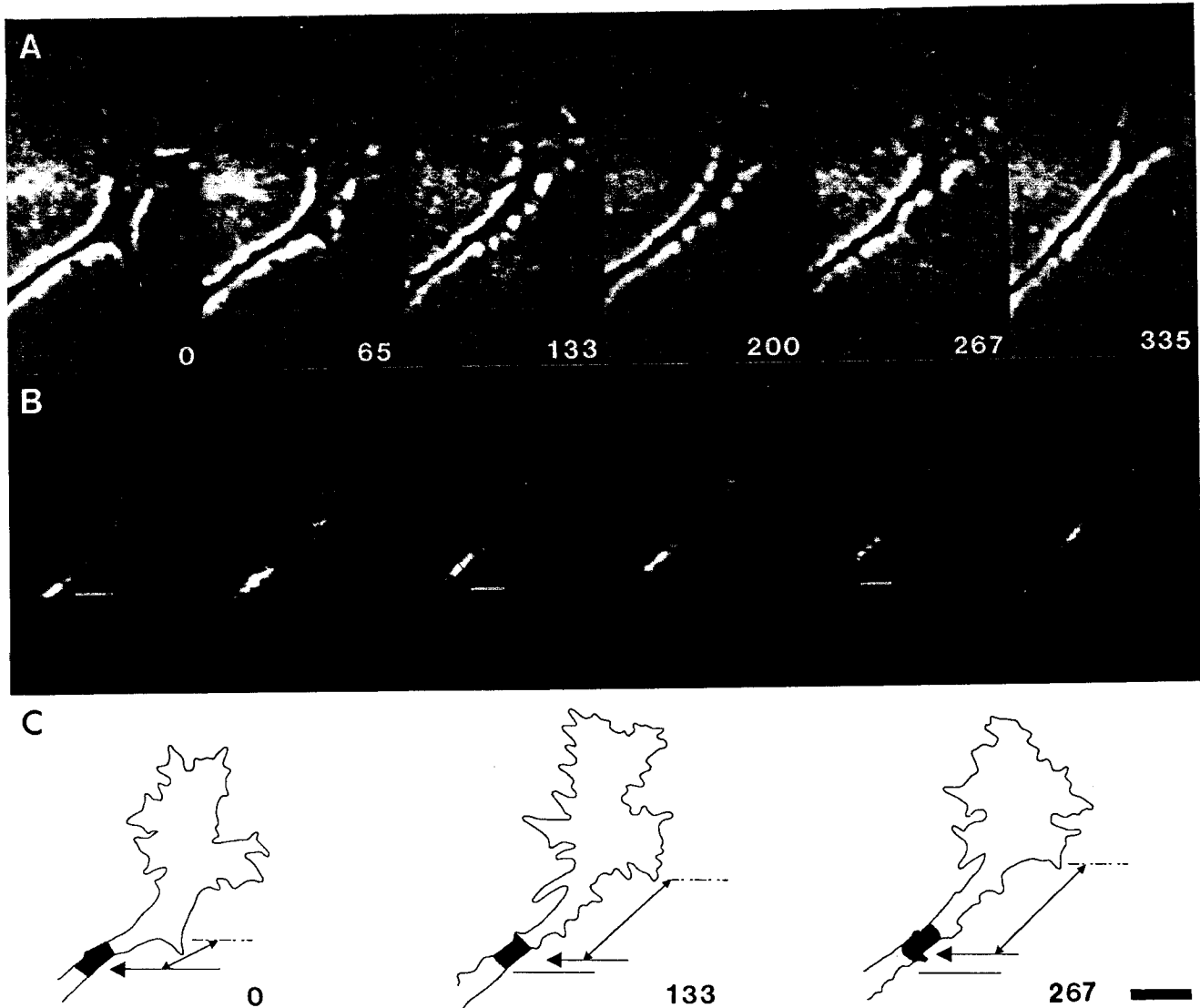


Figure 9. Coordination of polymer movement with growth cone movement: growth cone conversion. Phase images (A) and corresponding fluorescence images (B) at the times indicated (minutes) after photoactivation. (C) Tracing with superimposed fluorescein signal and phase outline of the growth cone from panels 1, 3, and 5. Note the rapid increase in distance (\longleftrightarrow) between photoactivation mark (arrow) and the neck of the growth cone (dashed line) between the first and third panels as the growth cone membrane collapses proximally to form a new segment of axon. In the final panel of A and B, the photoactivation mark once again starts to move out with the growth cone as conversion is complete. Solid line indicates starting position of photoactivation mark. Bar, 10 μm .

such as dynein, plausibly could generate movement of the proper polarity (Paschal et al., 1987). While the observed rates of polymer movement are slower than the rates of dynein-generated movement observed *in vitro* (Paschal and Vallee, 1987), the physical load on such a motor might account for the slower rate of transport. However, if translocation is powered by a microtubule motor, against what stationary phase is this motor moving? Microtubules could move relative to other microtubules, as they do in cilia and flagella. If this is the case, we would have expected to see a stationary phase of photoactivated microtubules, which we did not observe. It is possible that the stationary phase is exceedingly small, and detection would require an imaging system with greater sensitivity than that used in these experiments. Other cytoskeletal components, such as cortical actin, are candidates for a stationary phase relative to which the microtu-

bules might move (Fath and Lasek, 1988; Hirokawa, 1982; Schnapp and Reese, 1982). However, all these components must be themselves transported (Black and Lasek, 1980) so that it seems that no components would be truly stationary and that some would equilibrate between stationary and moving phases.

We are deeply indebted to the Growth Cone Collective, that is, Elly Tanaka and James Sabry, for stimulating discussion and fruitful collaboration throughout the course of this project. Additional thanks to Elly Tanaka for providing the micrograph for Fig. 1 C. We thank Bill Theurkauf for critical reading of this manuscript, and David States for his unfailing support in this project.

These studies are supported by a grant from National Institutes of General Medical Science to Marc Kirschner; and funding from the Lucille Markey Foundation for the microscope and image analysis equipment. S. S. Reinsch is the recipient of a University of California President's

Fellowship. T. J. Mitchison is supported by grants from the Searle Foundation and the Packard Foundation.

Received for publication 17 May 1991 and in revised form 24 June 1991.

References

- Baas, P. W., and M. M. Black. 1990. Individual microtubules in the axon consist of domains that differ in both composition and stability. *J. Cell Biol.* 111:495-509.
- Bamburg, J. 1988. The axonal cytoskeleton: stationary or moving matrix? *TINS (Trends Neurosci.)* 11:248-249.
- Bamburg, J. R., D. Bray, and K. Chapman. 1986. Assembly of microtubules at the tip of growing axons. *Nature (Lond.)* 321:778-790.
- Black, M. 1986. Interval between the synthesis and assembly of cytoskeletal proteins in cultured neurons. *J. Neurosci.* 6:1004-1012.
- Black, M., and R. Lasek. 1980. Slow components of axonal transport: two cytoskeletal networks. *J. Cell Biol.* 86:616-623.
- Brady, S., and R. Lasek. 1982. Fast axonal transport in extruded axoplasm from squid giant axon. *Science (Wash. DC)* 218:1129-1131.
- Brady, S., R. Lasek, and R. Allen. 1982. Video microscopy of fast axonal transport in extruded axoplasm: a new model for study of molecular mechanisms. *Cell Motil.* 5:81-102.
- Bray, D., and M. B. Bunge. 1981. Serial analysis of microtubules of cultured rat sensory neurons. *J. Neurocytol.* 10:589-605.
- Fath, K. R., and R. J. Lasek. 1988. Two classes of actin microfilaments are associated with the inner cytoskeleton of axons. *J. Cell Biol.* 107:613-621.
- Gilson, C. A., N. Ackland, and B. Burnside. 1986. Regulation of reactivated elongation in lysed cell models of teleost retinal cones by cAMP and calcium. *J. Cell Biol.* 102:1047-1059.
- Gorbisky, G., and G. Borisy. 1989. Microtubules of the kinetochore fiber turn over in metaphase but not in anaphase. *J. Cell Biol.* 109:653-662.
- Gorbisky, G. J., P. J. Sammak, and G. G. Borisy. 1987. Chromosomes move poleward in anaphase along stationary microtubules that coordinately disassemble from their kinetochore ends. *J. Cell Biol.* 104:9-18.
- Harris, W. A., C. E. Holt, T. A. Smith, and N. Gallenson. 1985. Growth cones of developing retinal cells in vivo, on culture surfaces, and in collagen matrices. *J. Neurosci. Res.* 13:101-122.
- Hirokawa, N. 1982. Cross-linker system between neurofilaments, microtubules, and membranous organelles in frog axons revealed by the quick-freeze, deep-etching method. *J. Cell Biol.* 94:129-142.
- Hirokawa, N., and H. Yorifuji. 1986. Cytoskeletal architecture of reactivated crayfish axons, with special reference to crossbridges among microtubules and between microtubules and membrane organelles. *Cell Motil.* 6:458-468.
- Hirokawa, N., S. Hisanaga, and Y. Shiomura. 1988. MAP2 is a component of crossbridges between microtubules and neurofilaments in the neuronal cytoskeleton: quick-freeze, deep-etch immunoelectron microscopy and reconstitution studies. *J. Neurosci.* 8:2769-2779.
- Hoffman, P., and R. Lasek. 1975. The slow component of axonal transport. Identification of major structural polypeptides of the axon and their generality among mammalian neurons. *J. Cell Biol.* 66:351-366.
- Hollenbeck, P. J. 1989. The transport and assembly of the axonal cytoskeleton. *J. Cell Biol.* 108:223-227.
- Hyman, A., D. Drechsel, D. Kellog, S. Salsler, K. Sawin, P. Steffen, L. Wordeman, and T. J. Mitchison. 1990. Preparation of modified tubulins. *Methods Enzymol.* 196:478-485.
- Keith, C. H. 1987. Slow transport of tubulin in the neurites of differentiated PC12 cells. *Science (Wash. DC)* 235:337-339.
- Keith, C. H., and K. Blane. 1990. Sites of tubulin polymerization in PC12 cells. *J. Neurochem.* 54:1258-1268.
- Krafft, G., R. Cummings, J. Dizig, L. Brvenik, W. Sutton, and B. Wars. 1986. Fluorescence activation and photodissipation (FDP). In *Nucleocytoplasmic Transport*. R. Peters and M. Trendelenberg, editors. Springer-Verlag, New York. 35-52.
- Lang, I., M. Scholz, and R. Peters. 1986. Molecular mobility and nucleocytoplasmic flux in hepatoma cells. *J. Cell Biol.* 102:1183-1190.
- Lasek, R. 1986. Polymer sliding in axons. *J. Cell Sci (Suppl.)* 5:161-179.
- Lasek, R., J. Garner, and S. Brady. 1984. Axonal transport of the cytoplasmic matrix. *J. Cell Biol.* 99:212s-221s.
- Letourneau, P. 1982. Analysis of microtubule number and length in cytoskeletons of cultured chick sensory neurons. *J. Neurosci.* 2:806-814.
- Lim, S. S., P. J. Sammak, and G. G. Borisy. 1989. Progressive and spatially differentiated stability of microtubules in developing neuronal cells. *J. Cell Biol.* 109:253-263.
- Lim, S. S., K. J. Edson, P. C. Letourneau, and G. G. Borisy. 1990. A test of microtubule translocation during neurite elongation. *J. Cell Biol.* 111:123-130.
- Luby-Phelps, K., D. L. Taylor, and F. Lanni. 1986. Probing the structure of cytoplasm. *J. Cell Biol.* 102:2015-2022.
- Matsumoto, T. 1920. The granules, vacuoles, and mitochondria in the sympathetic nerve-fibers cultivated in vitro. *Johns Hopkins Hosp. Bull.* 31:91-93.
- Mitchison, T. 1989. Polewards microtubule flux in the mitotic spindle: evidence from photoactivation of fluorescence. *J. Cell Biol.* 109:637-652.
- Mitchison, T., and M. Kirschner. 1988. Cytoskeletal dynamics and nerve growth. *Neuron.* 1:761-772.
- Nakai, J. 1964. The movement of neurons in tissue culture. In *Primitive Motile Systems in Cell Biology*. R. Allen and N. Kamiya, editors. Academic Press, New York. 377-385.
- Okabe, S., and N. Hirokawa. 1988. Microtubule dynamics in nerve cells: analysis using microinjection of biotinylated tubulin into PC12 cells. *J. Cell Biol.* 107:651-664.
- Okabe, S., and N. Hirokawa. 1990. Turnover of fluorescently labeled tubulin and actin in the axon. *Nature (Lond.)* 343:479-482.
- Paschal, B. M., and R. B. Vallee. 1987. Retrograde transport by the microtubule-associated protein MAP 1C. *Nature (Lond.)* 330:181-183.
- Paschal, B. M., H. S. Shpetner, and R. B. Vallee. 1987. MAP 1C is a microtubule-activated ATPase which translocates microtubules in vitro and has dynein-like properties. *J. Cell Biol.* 105:1273-1282.
- Sawin, K. E., and T. J. Mitchison. 1991. Poleward microtubule flux mitotic spindles assembled in vitro. *J. Cell Biol.* 112:941-954.
- Schnapp, B., and T. Reese. 1982. Cytoplasmic structure in rapid-frozen axons. *J. Cell Biol.* 94:667-679.
- Schroer, T., and M. Sheetz. 1991. Functions of microtubule-based motors. *Annu. Rev. Physiol.* 53:629-652.
- Schulze, E., and M. Kirschner. 1986. Microtubule dynamics in interphase cells. *J. Cell Biol.* 102:1020-1031.
- Shpetner, H., and R. Vallee. 1989. Identification of dynamin, a novel mechanochemical enzyme that mediates interactions between microtubules. *Cell.* 59:421-432.
- Tanaka, E., and M. Kirschner. 1991. Microtubule behavior in the growth cones of living neurons during axon elongation. *J. Cell Biol.* 115:345-363.
- Vale, R. D. 1987. Intracellular transport using microtubule-based motors. *Annu. Rev. Cell Biol.* 3:347-378.
- Warren, R., and B. Burnside. 1978. Microtubules in cone myoid elongation in the teleost retina. *J. Cell Biol.* 78:247-259.
- Weisenberg, R. C., J. Flynn, B. C. Gao, S. Awodi, F. Skee, S. R. Goodman, and B. M. Riederer. 1987. Microtubule gelation-contraction: essential components and relation to slow axonal transport. *Science (Wash. DC)* 238:1119-1122.
- Weisenberg, R. C., J. Flynn, B. C. Gao, and S. Awodi. 1988. Microtubule gelation-contraction in vitro and its relationship to component of slow axonal transport. *Cell Motil. Cytoskeleton.* 10:331-340.
- Weiss, P., and H. Hiscoe. 1948. Experiments on the mechanism of nerve growth. *J. Exp. Zool.* 107:315-396.